Received: 27 January 2023 | Accepted: 24 June 2023

DOI: 10.1097/HC9.0000000000000247

ORIGINAL ARTICLE

OPEN

The role of intestine in metabolic dysregulation in murine Wilson disease

Gaurav V. Sarode[1] | Tagreed A. Mazi[2] | Kari Neier[3] | Noreene M. Shibata[1] | Guillaume Jospin[4] | Nathaniel H.O. Harder[5] | Amanda Caceres[5] | Marie C. Heffern[5] | Ashok K. Sharma[6] | Shyam K. More[7] | Maneesh Dave[1] | Shannon M. Schroeder[1] | Li Wang[8] | Janine M. LaSalle[3] | Svetlana Lutsenko[8] | Valentina Medici[1]

[1]Department of Internal Medicine, Division of Gastroenterology and Hepatology, UC Davis, Sacramento, California, USA

[2]Department of Community Health Sciences - Clinical Nutrition, College of Applied Medical Sciences, King Saud University, Riyadh, Saudi Arabia

[3]Department of Medical Microbiology and Immunology, UC Davis School of Medicine, Genome Center, MIND Institute, Davis, California, USA

[4]AnimalBiome

[5]Department of Chemistry, University of California Davis Genome Center, Davis, California, USA

[6]Department of Gastroenterology, Inflammatory Bowel & Immunology Research Institute, Cedars Sinai Medical Center, Los Angeles, California, USA

[7]Cedars Sinai Medical Center, F. Widjaja Foundation Inflammatory Bowel Disease Institute, Department of Medicine, Cedars-Sinai Medical Center, Los Angeles, California, USA

[8]Department of Physiology, Johns Hopkins University, School of Medicine, Baltimore, Maryland, USA

Correspondence
Valentina Medici, Department of Internal Medicine, Division of Gastroenterology and Hepatology, University of California, Davis, 4150 V Street, Suite 3500, Sacramento, CA 95817, USA.
Email: vmedici@ucdavis.edu

Abstract

Background: The clinical manifestations of Wilson disease (WD) are related to copper accumulation in the liver and the brain, but little is known about other tissue involvement regarding metabolic changes in WD. *In vitro* studies suggested that the loss of intestinal ATP7B affects metabolic dysregulation in WD. We tested this hypothesis by evaluating the gut microbiota and lipidome in 2 mouse models of WD and by characterizing a new mouse model with a targeted deletion of *Atp7b* in the intestine.

Methods: Cecal content 16S sequencing and untargeted hepatic and plasma lipidome analyses in the Jackson Laboratory toxic-milk and the *Atp7b* null global knockout mouse models of WD were profiled and integrated. Intestine-specific *Atp7b* knockout mice ($Atp7b^{\Delta IEC}$) were generated and characterized using targeted lipidome analysis following a high-fat diet challenge.

Abbreviations: APOB, apolipoprotein B; $Atp7b^{-/-}$, *Atp7b* null global knockout mouse on a hybrid background; $Atp7b^{\Delta IEC}$, intestine-specific *Atp7b* knockout mouse; C3H, The Jackson Laboratory C3HeB/FeJ; DGs, diglycerides; FA, fatty acid; HFD, high-fat diet; IEC, intestinal epithelial cell; iWT, $Lox^{+/+}$/Cre; littermate control for $Atp7b^{\Delta IEC}$ mice; KO, *Atp7b* null global knockout mouse on a C57Bl/6 background; LPCs, lysophosphatidylcholines; PCs, phosphatidylcholines; PCA, principal component analysis; PE, phosphatidylethanolamine; PEMT, PE N-methyltransferase; PLs phospholipids; PPAERα, peroxisome-proliferator-activated receptor alpha; PUFAs, polyunsaturated fatty acids; SMs, sphingomyelins; SREBP1c, sterol regulatory element-binding protein; TAGs, triacylglycerides; TGs, triglycerides; tx-j, The Jackson Laboratory toxic-milk mouse; VLCFA, very-long-chain fatty acid; WD, Wilson disease; WT, $Atp7b^{+/+}$ littermate control for KO mice.

Supplemental Digital Content is available for this article. Direct URL citations are provided in the HTML and PDF versions of this article on the journal's website, www.hepcommjournal.com.

Results: Gut microbiota diversity was reduced in animal models of WD. Comparative prediction analysis revealed amino acid, carbohydrate, and lipid metabolism functions to be dysregulated in the WD gut microbial metagenome. Liver and plasma lipidomic profiles showed dysregulated triglyceride and diglyceride, phospholipid, and sphingolipid metabolism in WD models. However, *Atp7b*$^{\Delta IEC}$ mice did not show gut microbiome differences compared to wild type. When challenged with a high-fat diet, *Atp7b*$^{\Delta IEC}$ mice exhibited profound alterations to fatty acid desaturation and sphingolipid metabolism pathways as well as altered APOB48 distribution in intestinal epithelial cells.
Conclusions: Gut microbiome and lipidome underlie systemic metabolic manifestations in murine WD. Intestine-specific ATP7B deficiency affected both intestinal and systemic response to a high-fat challenge but not the microbiome profile, at least at early stages. WD is a systemic disease in which intestinal-specific ATP7B loss and diet influence the phenotype and the lipidome profile.

INTRODUCTION

Wilson disease (WD) is a rare disease characterized by a spectrum of hepatic and neuropsychiatric clinical manifestations with a varied severity. The traditional and established view of WD pathogenesis is rooted in the role of the copper-transporting ATPase beta (ATP7B), as mutations in the *ATP7B* gene cause WD. The *ATP7B* disease-causing variants have lost or greatly diminished copper transport activity, and copper accumulates in hepatocytes, leading to cellular and systemic metabolic alterations including oxidative stress, mitochondrial changes, and perturbed lipid and methionine metabolism.[1–3] Previous untargeted metabolite profiling revealed altered phospholipid (PL) levels in patients with WD, which were corroborated by findings in a mouse model of WD.[4,5] Fatty liver is a frequent manifestation of WD, occurring mostly in the absence of obesity and other features of metabolic syndrome. Diet has emerged as a key modulator of WD pathogenesis. An obesogenic diet with high fructose corn syrup and high sucrose content induces alterations in both lipid profiles and parameters of copper metabolism.[6] In a rat model of WD, feeding a high-calorie western diet exacerbated mitochondria dysfunction, hepatic steatosis, and liver damage.[3]

Murine models of WD play a crucial role in the understanding of its pathogenesis as they reliably accumulate copper and develop hepatic histological manifestations resembling human liver disease. *Atp7b* null mice maintained on different backgrounds (hybrid or C57Bl/6) consistently showed similar lipid metabolism changes,[7] despite different rates of copper accumulation. The *Atp7b* null global knockout model on a hybrid C57BL/6 × 129S6/SvEv background (*Atp7b*$^{-/-}$) has metabolic phenotypes, including impaired cholesterol synthesis pathways similar to those described in patients with WD.[8] This mouse model was also shown to have improved insulin sensitivity and blunted weight gain in response to a 10-week course of western diet.[9] The Jackson Laboratory toxic-milk mouse C3He-Atp7b$^{tx\text{-}J}$/J (tx-j), characterized by a spontaneous mutation of *Atp7b* and hepatic copper accumulation, also has altered lipid metabolism that partially overlaps with findings in WD patients.[10]

Although the primary sites of WD clinical manifestations are the liver and brain, growing evidence indicates multiple organs are affected, including the intestine, heart, and kidneys. However, it remains unknown whether the involvement of extrahepatic organs is independent of liver defects or secondary to hepatic copper accumulation. The ATP7B tissue-specific roles are also largely unknown. A role of ATP7B in intestinal epithelial cells (IECs), gut lipid metabolism, and chylomicron maturation was demonstrated in a groundbreaking study using intestine-derived organoids from *Atp7b*$^{-/-}$ mice.[11] Therefore, it is possible the inactivation of ATP7B in extrahepatic tissues, such as the intestine, directly contributes to systemic manifestations of WD, independent of hepatic copper accumulation, and severe hepatic pathological changes.

Given that both copper and lipid metabolism occur in the liver and IECs, it is likely that dietary factors and the gut microbiome have an effect on systemic WD energy metabolism with consequent impacts on the risk of developing hepatic steatosis and liver damage. In addition, initial studies in patients with WD indicate reduced alpha diversity of their gut microbiome.[12] Our

untargeted metabolomic profile in WD revealed a complex metabolic interaction involving dietary and microbiome-derived metabolites or metabolites for which plasma levels are affected by microbiome composition.[10]

The goal of the present study is to better understand the role of intestine in WD metabolic dysregulation. To reach this goal, we used a multipronged approach: the gut microbiome and lipidome were profiled in 2 mouse models of WD. Results were integrated and then mechanistically validated in a newly generated intestine-specific *Atp7b* knockout mouse model (*Atp7b*$^{\Delta IEC}$). This new model allowed us to study the impact of intestine ATP7B on lipid and copper metabolism independent of hepatic copper accumulation and advanced liver disease. Taken together, our data provide clear evidence of the important role intestine plays in WD pathogenesis, thus augmenting the current paradigm.

METHODS

Atp7b$^{\Delta IEC}$ model generation

Atp7b$^{\Delta IEC}$ mice were generated by the University of California Davis Mouse Biology Program using B6.Cg-Tg(Vil1-cre)997Gum/J mice from the Jackson Laboratory and *Atp7b*$^{Lox/Lox}$ mice [13] kindly provided by Dr. Svetlana Lutsenko (Johns Hopkins University). Cre-mediated removal of a 1.6-kb fragment in exon 2 results in IEC-specific *Atp7b* inactivation. Gene and protein expression were performed to confirm IEC-specific *Atp7b* inactivation (Supplemental Figure S1, http://links.lww.com/HC9/A480).

Experimental animals

All protocols were approved by the UC Davis Institutional Animal Care and Use Committee and follow the National Research Council's Guide for the Care and Use of Laboratory Animals as well as the ARRIVE guidelines. The *Atp7b* null global knockout on a C57Bl/6 background was generated as described;[13] this model will hereafter be referred to as "KO" to distinguish it from the hybrid background model. The KO model on a C57Bl/6 background was used for the present study as the development of their liver pathology resembles the natural history of the tx-j mouse. KO, *Atp7b*$^{\Delta IEC}$, tx-j, and C3HeB/FeJ (C3H) colonies were bred and maintained on the UC Davis campus in standard, open-top, plastic shoebox cages with Teklad TEK-Fresh bedding (Envigo, Madison, WI) and nesting enrichment material under the following conditions: 20°C–23°C, 40%–65% relative humidity, 14 h light/10 h dark light-cycle, and *ad libitum* LabDiet 5001 (PMI, St. Louis, MO) and deionized water. Mice were housed 2-4 per cage. Tx-j and C3H control were maintained as homozygous colonies. Homozygous tx-j dams have deficient copper levels in their milk for supporting growth and development; tx-j pups must be fostered to a dam with normal milk, otherwise they will die from copper deficiency within 14 days postpartum. Tx-j pups were cross-fostered to a C3H dam in the same phase of lactation as the biological tx-j dam between 3 and 5 days postpartum and were raised alongside the C3H dam's biological pups of the same age. Tx-j and C3H mice were segregated by genotype and sex at weaning. Knockout colonies were maintained by hemizygous (*Atp7b*$^{\Delta IEC}$) or heterozygous (KO) breeding to generate littermate controls. KO and *Atp7b*$^{\Delta IEC}$ mice were co-housed with their respective littermate controls and segregated by sex at weaning. Additional study details and experimental methods can be found in Supplemental Material, http://links.lww.com/HC9/A480.

RESULTS

These studies employed 2 mouse models of WD: tx-j mice on a C3H genetic background and KO mice on a C57Bl/6 background. Tx-j mice have an inactivating mutation in *Atp7b*, whereas KO mice are a global knockout with ATP7B protein expression lacking in all tissues. Despite genetic differences, both animal models accumulate copper in the liver and show similar natural history of liver disease progression. As shown in Supplemental Table S3, http://links.lww.com/HC9/A480, at 16 weeks of age, tx-j mice presented significantly lower body weight compared to age-matched control C3H mice with normal copper metabolism, as described;[14] KO body weights were not different from *Atp7b*$^{+/+}$ littermate controls (WT) of the same sex. As expected, female mice of both strains had lower body weight compared to their male counterparts. However, liver-per-body-weight was significantly higher in female tx-j mice compared with either C3H control or male tx-j mice. This difference was not observed for the KO animals. Mesenteric-white-adipose-tissue-per-body-weight was significantly lower in tx-j mice compared with control but was not different between KO and WT mice.

Systemic loss of *Atp7b* impacts gut microbiome

To examine changes in the intestinal microbiome associated with *Atp7b* mutation prior to advanced liver disease, microbiome profiling was conducted on 16-week-old mice (Supplemental Figure S2, http://links.lww.com/HC9/A480 for study design). At this age, both tx-j and KO mice already accumulate copper in the liver [7,15–17] and, although they do not yet show significant hepatic steatosis or fibrosis (Supplemental Figure S3, http://links.

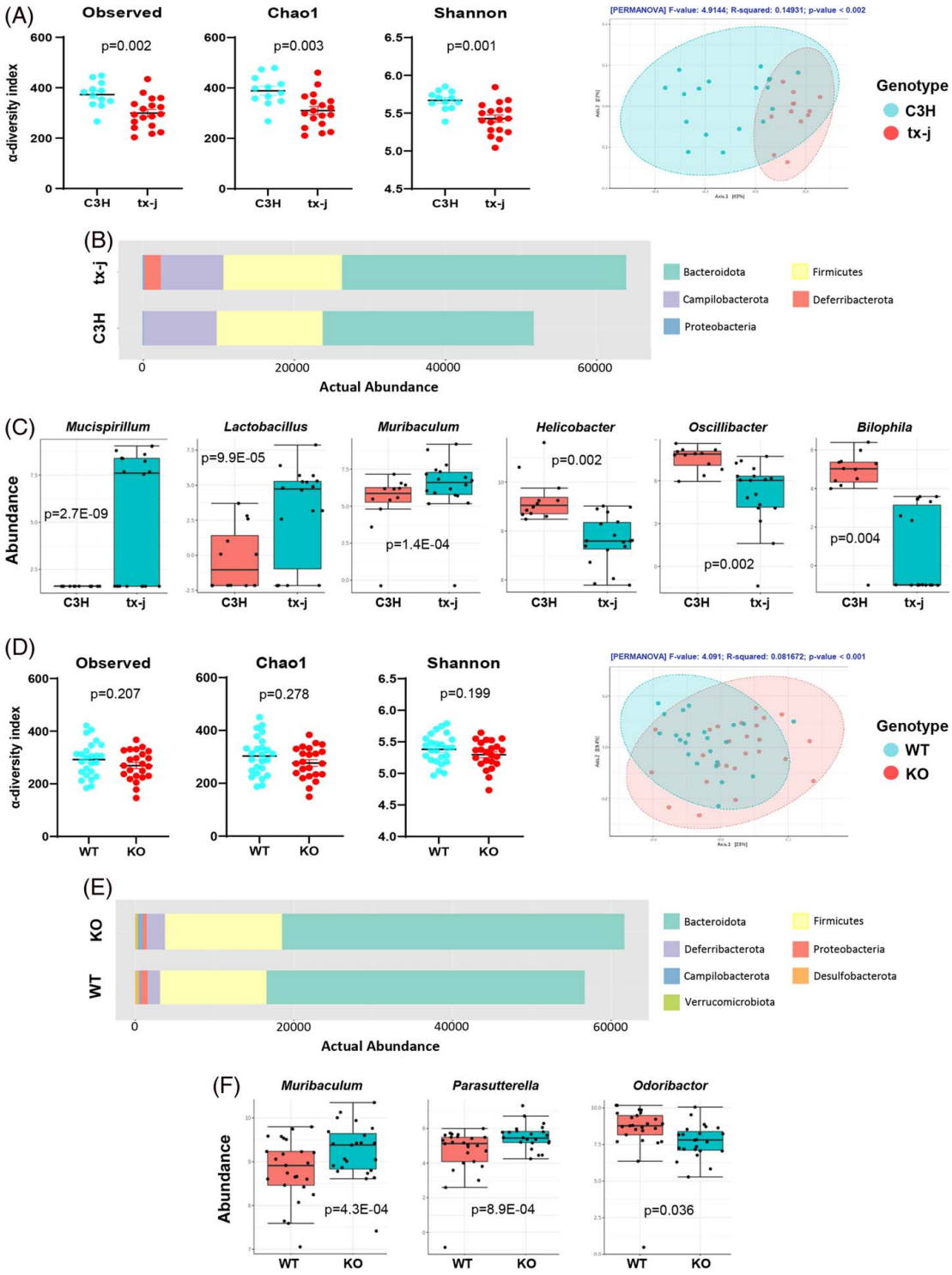

FIGURE 1 Composition and structure of cecal content microbiota profiles in 16-week-old tx-j versus C3H and KO versus WT mice. (A, D) Alpha-diversity analysis shown as observed species richness, Chao1 index, and Shannon index. Scatter plots are shown as the mean ± SD. Microbial beta-diversity was accessed by NMDS analysis based on Bray-Curtis dissimilarity index by permutational multivariate ANOVA. (B, E) Microbial abundance at the phylum level. (F) Box plots representing the relative abundance of the top significantly altered bacteria at the genus level. tx-j (n = 18), C3H (n = 13), KO (n = 23), and WT (n = 23) mice. Abbreviations: KO, knockout; WT, wild type.

lww.com/HC9/A480), mice of both strains present markedly enlarged hepatocyte nuclei with cytosolic glycogenosis and mild inflammatory infiltrate. Cecal content 16S sequencing revealed decreased alpha diversity of the tx-j microbiome when compared with C3H control, as estimated by observed species index ($p = 0.002$), Chao1 index ($p = 0.003$), and Shannon index ($p = 0.001$) (Figure 1A). Beta-diversity analysis (Figure 1B)

demonstrated significant partitioning of bacterial communities ($F = 4.9355$; $R^2 = 0.1499$; $p < 0.002$).

Comparison of gut microbiota composition at the phylum and genus levels in tx-j versus C3H mice found that differences in 5 bacterial phyla (Bacteroidota, Campilobacterota, Deferribacterota, Firmicutes, and Proteobacteria) were dominant (Figure 1C). In the taxonomic profile for tx-j versus C3H, the operational taxonomic units were assigned to prevalent microbiome components of the phyla Bacteroidota (53% vs. 46%), Firmicutes (32% vs. 39%), Campilobacterota (10% vs. 14%), and Deferribacterota (4% vs. 1%) (Supplemental Figure S4, http://links.lww.com/HC9/A480). A clustered heat map showing the variation of taxonomic abundance at the genus level by genotype and sex in tx-j versus C3H is presented in Supplemental Figure S6, http://links.lww.com/HC9/A480.

The proportions of tx-j gut bacteria at the genus level were very distinct from those in C3H control mice. A total of 26 genera were identified of which 10 showed significant abundance differences according to classical univariate analysis ($p < 0.05$) (Supplemental Table S4, http://links.lww.com/HC9/A480). The relative abundances of Mucispirillum, Lactobacillus, Muribaculum, Rikenellaceae RC9 gut group, and Odoribacter were significantly higher in tx-j mice compared with C3H. *Helicobacter*, *Oscillibacter*, *Bilophila*, *Blautia*, and *Alistipes* were less abundant; however, they did not retain significance with FDR correction. The top 6 differential genera are shown in Figure 1D. Thus, systemic copper misbalance has a significant effect on the mouse gut microbiome.

Mouse genetic background modulates microbiome response

Analysis of alpha and beta diversity using 16S sequencing demonstrated that KO mice showed similar trends compared to changes seen in tx-j mice versus control, but differences were not statistically significant (Figure 1D). In KO versus WT groups, 7 bacterial phyla (Bacteroidota, Campilobacterota, Deferribacterota, Firmicutes, Proteobacteria, and Verrucomicrobiota) were dominant (Figure 1E). Twenty-three genera were identified with only *Muribaculum*, *Parasutterella*, *Bacteroides*, and *Desulfovibrio* presenting significantly higher abundances in KO mice compared with WT, and *Odoribacter* less abundant (Figure 1F, Supplemental Table S5, http://links.lww.com/HC9/A480). Bacterial phyla analysis did not show differences between KO and WT mice (Supplemental Figure S5, http://links.lww.com/HC9/A480). Overall, KO mice demonstrated microbiome differences in the same direction as tx-j mice but with fewer significant results. Thus, hepatic copper misbalance affects gut microbiome, though specific responses were strain dependent.

Functional metagenome predicts involvement of energy metabolism

To understand the microbiome's functional composition, we performed a comparative prediction analysis of the functional metagenome using PICRUSt. MicrobiomeAnalyst was used to map the abundance profile for functional analysis of microbiota. Unsupervised clustering by principal component analysis (PCA) showed the tx-j microbiota profile separated from that of C3H mice and with 44.8% of variance between the groups (Supplemental Figure S7, http://links.lww.com/HC9/A480). Moreover, classical univariate analysis identified 1957 significant KEGG orthology groups between tx-j and C3H mice. According to a KEGG metabolic network pathway analysis (Supplemental Table S6, http://links.lww.com/HC9/A480), the observed KEGG orthology shows primary involvement of energy metabolism including amino acid biosynthesis, metabolism of branched-chain amino acids, pyruvate metabolism, and the tricarboxylic acid cycle. In accordance with less pronounced differences in microbiome patterns for KO versus WT, less marked associations between microbiome and energy metabolism were found in the KO mice; regardless, associations were in the same direction as tx-j mice confirming the roles of hepatic copper accumulation and genotype on influencing both microbiome and energy metabolism pathways.

Lipidome analyses of liver and plasma identify specific lipid changes in mouse models of WD

To examine the effect of ATP7B deficiency on energy metabolism pathways, we focused on lipid metabolism and compared the liver and plasma lipid profiles in 16-week-old tx-j and KO mice to their respective controls, when fed a standard chow diet. PCA indicated distinct clustering and separation between tx-j and C3H for both liver (Figure 2A) and plasma (Figure 2B) lipidomes. Enrichment analysis of lipid classes for liver (Figure 2C) and plasma (Figure 2D) showed lower triglycerides (TGs), diglycerides (DGs), PLs, and sphingomyelins (SMs) along with higher ceramides in tx-j mice compared with C3H control mice. Plasma levels of unsaturated and saturated fatty acids were lower in tx-j mice compared with C3H control.

The hepatic lipidome in tx-j mice was particularly characterized by changes in unsaturated lipid classes, including lower levels of several triacylglycerides (TAGs) and phosphatidylcholines (PCs) with an altered phosphatidylethanolamine (PE) profile, indicating dysregulated PL metabolism. The sphingolipid profile was affected by higher ceramides and altered SMs. In addition, hepatic very-long-chain fatty acid (VLCFA) pathways were aberrant (Figure 2E). Likewise, in

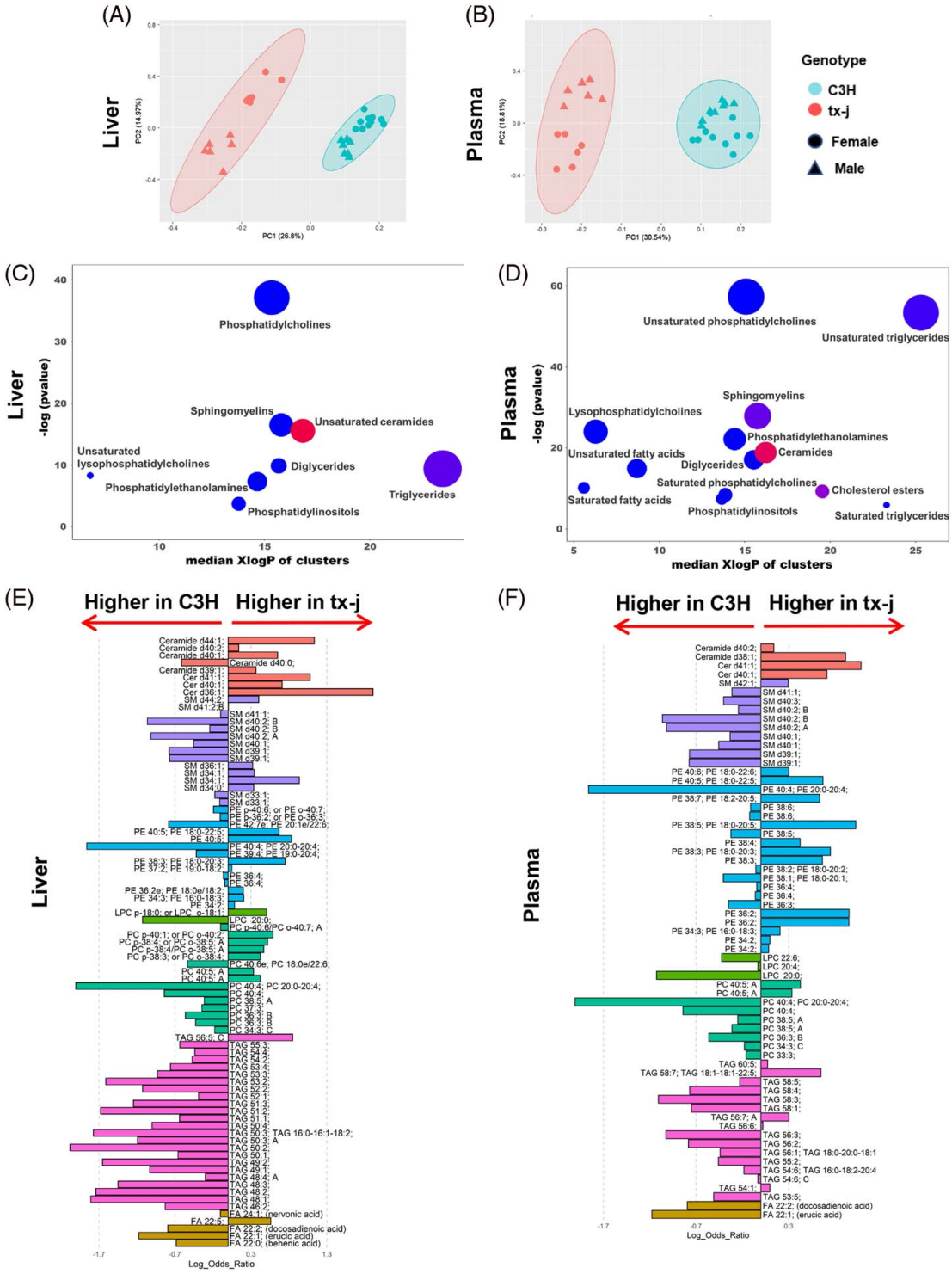

FIGURE 2 Lipidomic profiles in liver and plasma of tx-j mice compared with C3H control. (A, B) Principal component analysis based on the lipid profiling of tx-j mice and C3H control in liver and plasma. (C, D) Chemical similarity enrichment analysis (ChemRICH) and enrichment statistics plot for tx-j versus C3H mice in liver and plasma. Each cluster represents an altered chemical class of metabolites ($p < 0.05$). Cluster size represents the total number of metabolites. Cluster color represents the directionality of metabolite differences: red, higher in tx-j mice; blue, lower in tx-j mice. Colors in between refer to a mixed population of metabolites manifesting both higher and lower levels in tx-j mice when compared with C3H. The *x*-axis represents the cluster order on the chemical similarity tree. The *y*-axis represents chemical enrichment *p*-values calculated using a Kolmogorov-Smirnov test. (E, F) Linear discriminant analysis effect size (LEfSe) plot representing the logarithm of the ratios of the average levels of statistically different lipids between tx-j and C3H mice in liver and plasma. A positive log ratio bar indicates higher lipid levels in tx-j mice; a negative log ratio bar indicates higher levels in C3H mice. Colors represent lipids in the same class. tx-j (n = 18) and C3H (n = 13) mice. Abbreviations: FA, fatty acid; LPC, lysophosphatidylcholines; PE, phosphatidylethanolamine; TAG, triacylglycerides.

plasma, we observed altered TAGs and lower levels of many PCs and lysophosphatidylcholines (LPCs), with PE profile changes (Figure 2F). Higher ceramides, lower SMs, and altered VLCFAs were also observed. A list of all significantly altered metabolites is presented in Supplemental Material 2, http://links.lww.com/HC9/A481. Consistent with findings from the tx-j enrichment analysis and in accordance with less pronounced microbiome pattern differences, 16-week-old KO mice showed less separation in lipidomic profiles (Figure 3A, B) but had similar trends in liver and plasma lipidomic patterns compared with WT mice (Figure 3C–F).

Changes in gut microbiome correlate with changes in hepatic lipidome illustrating contribution to WD metabolic dysregulation

We then used the tx-j model to determine the association of microbiome profiles with hepatic lipidome. Specifically, we focused on microbiota genera exhibiting significant abundance and lipid classes showing significant differences in tx-j compared with C3H control (Figure 4A, B). With these criteria, we included 8 genera (*Mucispirillum*, *Lactobacillus*, *Muribaculum*, *Odoribacter*, *Bilophila*, *Oscillibacter*, *Helicobacter*, and *Blautia*) and selected hepatic TAGs, PLs, ceramides, SMs, and VLCFAs for correlation analysis (Supplemental Material 3, http://links.lww.com/HC9/A482). Similar criteria were used with lipid-microbe correlation analysis in KO versus WT (Figure 4C, D) and included 5 genera (*Muribaculum*, *Odoribacter*, *Desulfovibrio*, *Parasutterella*, and *Bacteroides*).

Many TAG species, such as TAG (46–58:1–5), were positively correlated with *Mucispirillum*, *Lactobacillus*, and *Blautia* ($r = 0.4$–0.6, FDR-adjusted $p < 0.05$). *Muribaculum*, *Lactobacillus*, *Odoribacter*, and *Blautia* were negatively associated with many PLs including PC (36–40:3–4) and PE(36–42:3–7); however, *Mucispirillum* was positively associated with many PLs including PC(40:4–6) and PE(34–40:2–5) ($r = 0.4$–0.7, FDR-adjusted $p < 0.05$). *Mucispirillum*, *Lactobacillus*, and *Blautia* were found to be negatively correlated with several SMs, including SM (33–41:1–2) ($r = 0.4$–0.7, FDR-adjusted $p < 0.05$). *Mucispirillum*, *Odoribacter*, and *Oscillibacter* were positively correlated with some ceramides, including Cer(d40–44:0–1) ($r = 0.4$–0.7, FDR-adjusted $p < 0.05$). Together, the correlations observed between *Mucispirillum*, *Muribaculum Lactobacillus*, and lipids classes, such as PLs and SMs, are in accordance with the direction of change observed in lipidomic profiles of tx-j and KO mice. Using a system-based approach to explore the liver data in more depth, we performed a weighted gene correlation network analysis of the microbiome and liver lipidome data of tx-j and KO mice. Through this analysis, a network of liver lipids for both tx-j and KO mice was constructed and organized in color-coded modules (Supplemental Figure S8, http://links.lww.com/HC9/A480 and related table with lipid membership in each module). With this unbiased approach, we similarly identified major lipid modules associated with WD in both tx-j and KO when compared with respective controls. Next, we studied genera-module associations in tx-j mice, focusing on *Mucispirillum*, given its previously described central association with metabolic changes characteristic of fatty liver. Liver lipid modules midnight blue, green yellow, green, and black were all significantly associated with *Mucispirillum*, particularly pointing to PC and LPC as identified associated lipids (Supplemental Figure S9, http://links.lww.com/HC9/A480).

To directly examine metabolic consequences of *Atp7b* inactivation in intestine alone, we generated a new mouse strain, *Atp7b*$^{\Delta IEC}$, with *Atp7b* deleted in enterocytes using Cre-recombinase under a villin-1 promoter. Alpha and beta diversity in gut microbiome of *Atp7b*$^{\Delta IEC}$ mice were not different compared with their Lox$^{+/+}$/Cre-littermate controls (iWT) (Supplemental Figure S10, http://links.lww.com/HC9/A480). No significant differences were observed in the abundance of genera between the iWT and *Atp7b*$^{\Delta IEC}$ mice groups, as shown in Supplemental Table S7, http://links.lww.com/HC9/A480.

No difference in hepatic copper concentration was observed between *Atp7b*$^{\Delta IEC}$ and iWT mice (Supplemental Figure S11, http://links.lww.com/HC9/A480). RNA-sequencing analysis revealed changes in lipid metabolism pathways, including fatty acid metabolism in the IECs of KO mice (Figure 5A, Table 1, Tables S8 and S9, http://links.lww.com/HC9/A480), whereas *Atp7b*$^{\Delta IEC}$ mice showed a smaller number of differentially expressed genes and predominantly changes in transcript levels of genes related to RNA synthesis, epigenetic regulation of gene expression, synthesis of bile salts, and various CYP450 enzymes involved in oxidation of organic compounds and lipid metabolism (Figure 5B, Table 1, Supplemental Table S10, http://links.lww.com/HC9/A480).

Lipid metabolism is altered in IECs of mice with a targeted *Atp7b* deletion

Since global inactivation of *Atp7b* impacts lipid metabolism, we challenged *Atp7b*$^{\Delta IEC}$ mice with an 8-day high-fat diet (HFD) to screen an acute response and investigate whether the atypical localization of APOB previously described in *Atp7b*$^{-/-}$ intestinal organoids [11] is recapitulated in *Atp7b*$^{\Delta IEC}$ IECs, further validating the model. At 9 weeks of age, *Atp7b*$^{\Delta IEC}$ body weights did not differ from iWT on chow or either genotype on HFD (Supplemental Table S11, http://links.lww.com/HC9/A480). However, chow-fed *Atp7b*$^{\Delta IEC}$ liver-per-body

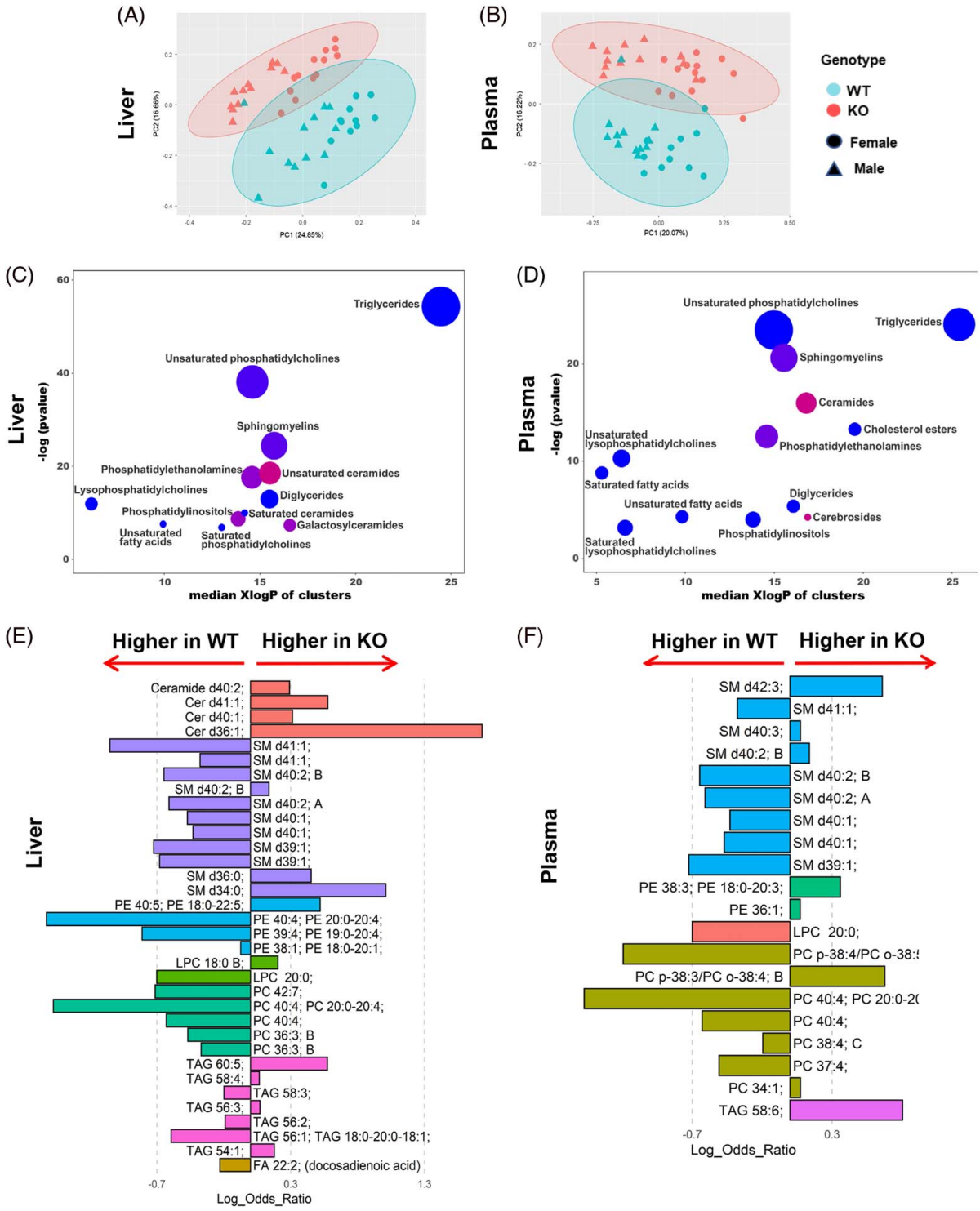

FIGURE 3 Lipidomic profiles in liver and plasma of KO mice compared with WT control. (A, B) Principal component analysis based on the lipid profiling of KO mice and WT control in liver and plasma. (C, D) Chemical similarity enrichment analysis (ChemRICH) and enrichment statistics plot for KO versus WT mice. Each cluster represents an altered chemical class of metabolites ($p < 0.05$). Cluster size represents the total number of metabolites. Cluster color represents the directionality of metabolite differences: red, higher in KO mice; blue, lower in KO mice. Colors in between refer to a mixed population of metabolites manifesting both higher and lower levels in KO mice when compared with WT. The *x*-axis represents the cluster order on the chemical similarity tree. The *y*-axis represents chemical enrichment *p*-values calculated using a Kolmogorov-Smirnov test. (E, F) Linear discriminant analysis effect size (LEfSe) plot representing the logarithm of the ratios of the average levels of statistically different lipids between KO and WT mice in liver and plasma. A positive log ratio bar indicates higher lipid levels in KO mice; a negative log ratio bar indicates higher levels in WT mice. Colors represent lipids in the same class. KO (n = 23) and WT (n = 23) mice. Abbreviations: FA, fatty acid; KO, knockout; LPC, lysophosphatidylcholines; PE, phosphatidylethanolamine; TAG, triacylglycerides; WT, wild type.

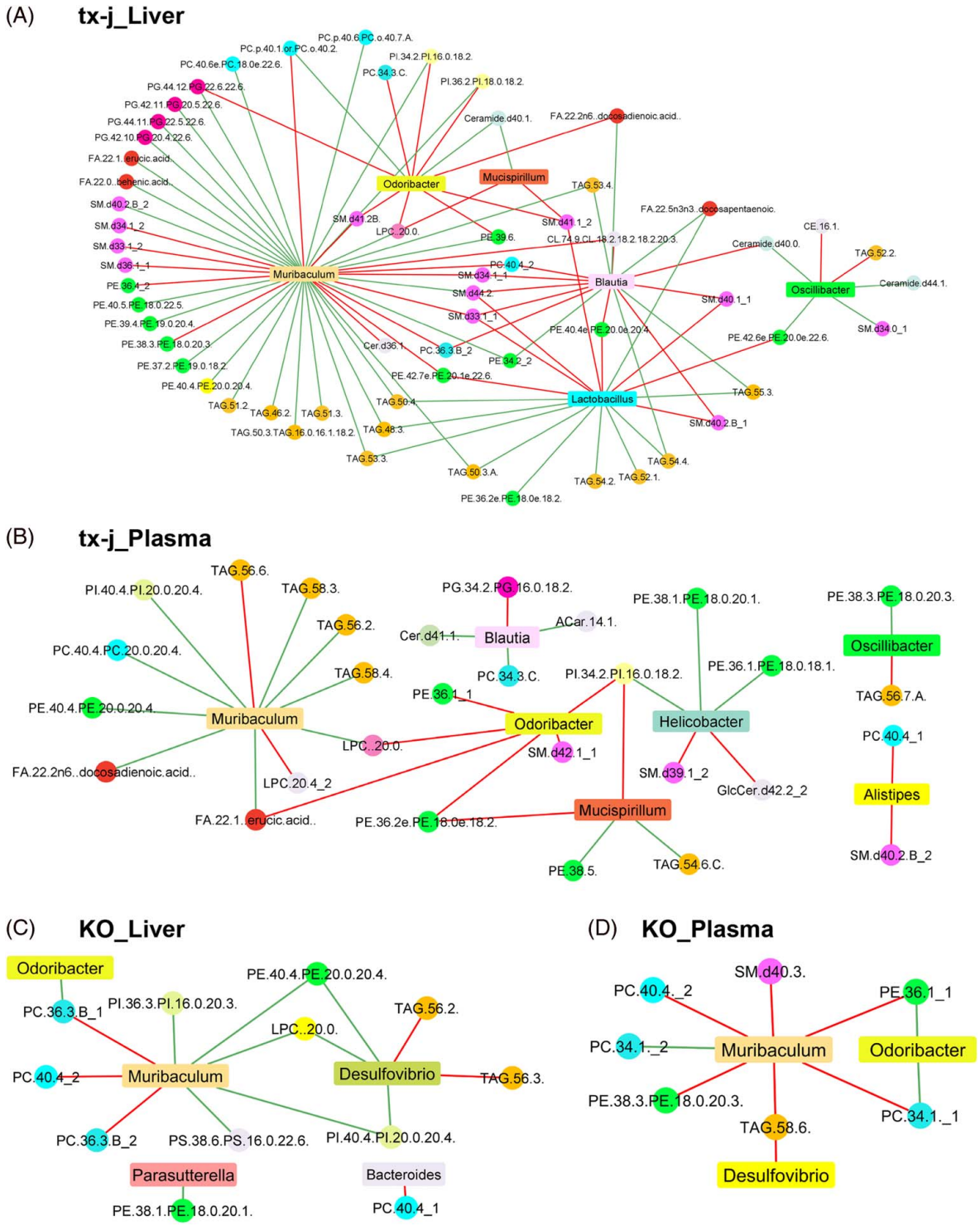

FIGURE 4 Microbe-metabolite network plots for liver and plasma of tx-j and KO mice. (A, B) Microbe-metabolite relational networks showing all significant bacterial genus-lipid metabolite pairs ($p \leq 0.05$) between liver and plasma of tx-j and C3H mice. (C, D) Microbe-metabolite relational networks showing all significant bacterial genus-lipid metabolite pairs ($p \leq 0.05$) between liver and plasma of KO and WT mice. Compositionally corrected correlations (calculated using CCREPE function in *R*) between microbial taxa and metabolite intensities were used to generate the network plots in CytoScape. In the network plot, the color of the lines represents positive (green) or negative (red) correlations. Nodes of the network represent microbial taxa (rectangle) and lipids (circle); lipid nodes with the same color belong to the same lipid class. Abbreviations: PC, phosphatidylcholine; PE, phosphatidylethanolamine; SM, sphingomyelin; TAG, triacylglycerides.

weight ratios were significantly higher than iWT chow or either genotype on HFD. As a comparison for the knockout construct, a few KO and WT mice were also given the 8-day HFD challenge. Body weights did not differ between genotypes and diets but liver-per-body-weight ratios were significantly lower in KO and WT

TABLE 1 RNA-sequencing pathway analysis of KO vs. WT and *Atp7b*$^{\Delta IEC}$ vs. iWT

REACTOME pathway	*p*	Total no. genes	Total # of upregulated genes	Total no. downregulated genes
KO vs. WT				
Metabolism of steroids	1.30E-06	28	26	2
Cholesterol biosynthesis	9.24E-06	11	11	0
Gluconeogenesis	0.001229	9	8	1
Biological oxidations	0.002187	35	28	7
Bile acid and bile salt metabolism	0.003046	10	9	1
Scavenging of heme from plasma	0.003921	7	5	2
Phase I—functionalization of compounds	0.004727	22	17	5
MHC class II antigen presentation	0.004996	19	10	9
Amplification of signal from the kinetochores	0.005185	17	0	17
Amplification of signal from unattached kinetochores by means of a MAD2 inhibitory signal	0.005185	17	0	17
HS-GAG degradation	0.006142	6	1	5
Metabolism of vitamins and cofactors	0.006906	26	19	7
Binding and uptake of ligands by scavenger receptors	0.007108	9	7	2
Mitotic prometaphase	0.008759	28	0	28
Synthesis of prostaglandins (PG) and thromboxanes (TX)	0.009567	5	5	0
Androgen biosynthesis	0.010068	4	4	0
The NLRP3 inflammasome	0.010068	4	2	2
Glucose metabolism	0.011159	14	10	4
Retinoid metabolism and transport	0.013889	9	5	4
ERBB2 activates PTK6 signaling	0.014668	4	2	2
Atp7b$^{\Delta IEC}$ vs. iWT				
Phase I—functionalization of compounds	0.000324	7	4	3
Biological oxidations	0.000508	9	5	4
Cytochrome P450—arranged by substrate type	0.001066	5	2	3
eNOS activation	0.004585	2	0	2
Xenobiotics	0.007638	3	0	3
Rap1 signaling	0.007788	2	1	1
Positive epigenetic regulation of rRNA expression	0.008	4	0	4
B-WICH complex positively regulates rRNA expression	0.008	4	0	4
Metabolism of nitric oxide	0.009024	2	0	2
eNOS activation and regulation	0.009024	2	0	2
Synthesis of bile acids and bile salts by means of 24-hydroxycholesterol	0.010343	2	2	0
Cellular responses to external stimuli	0.012357	10	2	8
Cellular responses to stress	0.012517	9	1	8
Epigenetic regulation of gene expression	0.016521	4	0	4
Endogenous sterols	0.021707	2	2	0
Aflatoxin activation and detoxification	0.021707	2	0	2
TNFs bind their physiological receptors	0.025591	2	1	1
RNA polymerase I chain elongation	0.034123	2	0	2

TABLE 1. (*continued*)

REACTOME pathway	*p*	Total no. genes	Total # of upregulated genes	Total no. downregulated genes
DNA damage/telomere stress-induced senescence	0.035068	3	0	3
RNA polymerase I promoter escape	0.036407	2	0	2

Notes: Top 20 pathways with differentially expressed genes.

mice on HFD. Liver histology of HFD-fed *Atp7b*$^{\Delta IEC}$ mice presented cytosolic glycogenosis and vacuolization similarly to chow-fed mice of the same genotype (Supplemental Figure S12, http://links.lww.com/HC9/A480). On chow, both iWT and *Atp7b*$^{\Delta IEC}$ enterocytes had an expected perinuclear targeting of APOB, consistent with its *trans*-Golgi localization (Figure 5C). In some animals, APOB staining in *Atp7b*$^{\Delta IEC}$ appeared more diffuse compared to iWT, but differences were subtle. However, after the 8-day HFD challenge, the difference between iWT and *Atp7b*$^{\Delta IEC}$ mice was very clear with APOB localization mostly in cytosolic vesicles in *Atp7b*$^{\Delta IEC}$ enterocytes, shown in Figure 5C (d). This pattern was similar to the aberrant vesicular distribution of APOB in the intestinal organoids derived from *Atp7b*$^{-/-}$ mouse.[11]

Lipidome analysis of *Atp7b*$^{\Delta IEC}$ liver demonstrates contribution of intestinal ATP7B to systemic metabolic dysregulation in WD

To understand the effect of intestine ATP7B removal on lipid metabolism independent from copper accumulation in the liver, we examined liver and plasma targeted lipidomic profiles in *Atp7b*$^{\Delta IEC}$ mice at 9 weeks of age, focusing on lipid classes that showed different abundances in the untargeted comparison of 16-week-old KO versus WT mice.

Compared to iWT, *Atp7b*$^{\Delta IEC}$ mice on chow showed subtle changes highlighting increased liver TGs, DGs, and unsaturated FAs (Figure 6A). In plasma, *Atp7b*$^{\Delta IEC}$ mice showed higher levels of lysoPCs and lysoPEs, and reduced SM and ceramides (Figure 6B). *Atp7b*$^{\Delta IEC}$ mice challenged with HFD showed distinct clustering and separation from iWT and chow-fed *Atp7b*$^{\Delta IEC}$ liver and plasma lipidomes as indicated by heat map (Supplemental Figure S13A, http://links.lww.com/HC9/A480) and PCA analysis (Supplemental Figure S13B, C, http://links.lww.com/HC9/A480). iWT mice fed a HFD also clearly separated from chow-fed iWT mice (Supplemental Figure S13D, E, http://links.lww.com/HC9/A480), indicating a role of genotype in the observed differences. Specifically, compared to iWT on the same HFD, *Atp7b*$^{\Delta IEC}$ mice responded with high hepatic unsaturated TGs and DGs and altered plasma TGs, SMs, and PLs (Figure 6C, D). Compared to chow-fed *Atp7b*$^{\Delta IEC}$ mice, *Atp7b*$^{\Delta IEC}$ mice on HFD presented a dramatic increase in hepatic TAGs and DGs, and lower acylcarnitines; HFD also resulted in altered ceramides and increased SMs as well as a dysregulated PL profile, with lower levels of many PCs and PEs, and altered lysoPCs and lysoPEs (Figure 6E). In plasma, *Atp7b*$^{\Delta IEC}$ on HFD resulted in lower TAGs and higher acylcarnitines, ceramides, and SMs (Figure 6F).

When comparing the effects of HFD on the lipidomes of KO mice, PCA indicated marginal separation between chow-fed and HFD-fed KO mice in both liver (Supplemental Figure S14A, http://links.lww.com/HC9/A480) and plasma (Supplemental Figure S14B, http://links.lww.com/HC9/A480). WT mice fed a HFD were distinctly separated from chow-fed WT mice (Supplemental Figure S14C, D, http://links.lww.com/HC9/A480), although the analysis is limited by the small number of mice. Compared to WT on HFD, KO mice fed a HFD presented increased unsaturated FA and DGs in liver (Figure 7A) and increased unsaturated TGs and ceramides in plasma (Figure 7B). Compared to chow, the KO hepatic lipidome showed increased DGs and a trend in increased TAGs (not FDR significant) on HFD (Figure 7C) in a similar direction compared to *Atp7b*$^{\Delta IEC}$ mice. Whereas no changes in hepatic ceramides were observed, the PL profile was found altered with lower levels of many PCs (Figure 7E). In plasma, the HFD challenge resulted in several decreased TAGs along with altered PL profiles and increased levels of ceramides and SMs (Figure 7D, F).

DISCUSSION

We conducted an integrated analysis of the microbiome and lipidome in animal models of WD and investigated the combined effects of intestine-specific *Atp7b* deficiency and HFD challenge, resulting in several novel findings. First, global *Atp7b* deficiency was characterized by lower microbiome diversity along with changes involving phyla and genera previously associated with liver disease and fatty liver in the general population. Second, global *Atp7b* deficiency was associated with altered lipidomic profiles in 2 mouse models of WD, specifically dysregulated hepatic fatty acid desaturation and SLs independent of severe liver disease. Third,

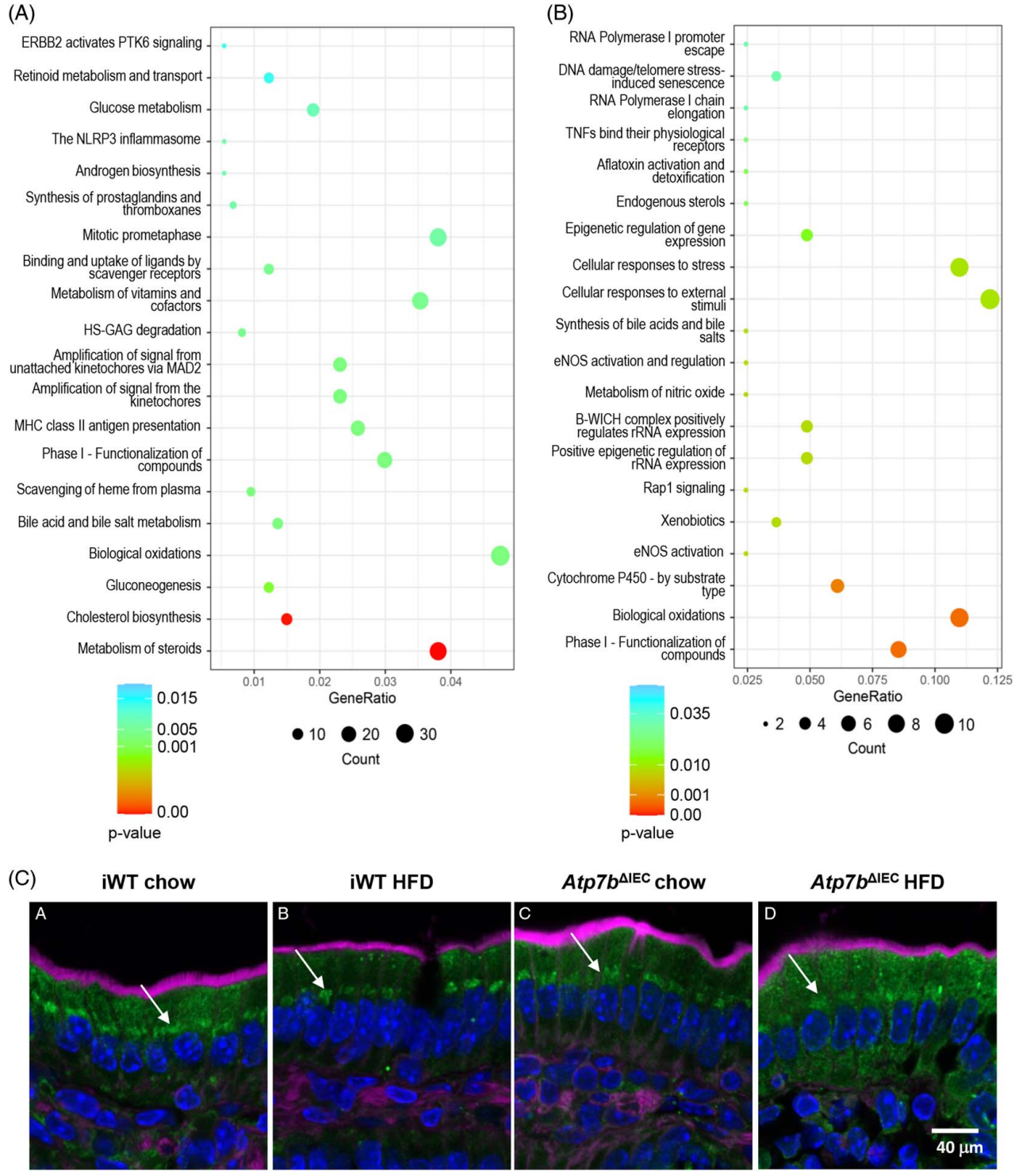

FIGURE 5 Pathway enrichment analysis and APOB distribution in *Atp7b*$^{\Delta IEC}$ mouse intestine. (A, B) REACTOME pathway analysis of RNA-seq data for KO versus WT and *Atp7b*$^{\Delta IEC}$ versus iWT, respectively, at 16 weeks of age. The plot represents the top 20 pathways with differentially expressed genes ($p < 0.05$). The dot size indicates the number of differentially expressed genes and the dot color represents *p*-value. KO (n = 6), WT(n = 6), *Atp7b*$^{\Delta IEC}$ (n = 6), and iWT(n = 6). C: Immunofluorescence for APOB48 in the intestine of iWT and *Atp7b*$^{\Delta IEC}$ mice fed chow or HFD at 9 weeks of age. APOB48 (green) presented similar perinuclear distribution (arrows) in iWT mice, regardless of the dietary fat content (A, B), and in *Atp7b*$^{\Delta IEC}$ mice fed chow (C). However, after HFD challenge in *Atp7b*$^{\Delta IEC}$ mice, APOB48 presented a diffuse cytosolic distribution indicating an impairment of chylomicron processing within the IECs (D). iWT chow (n = 3), *Atp7b*$^{\Delta IEC}$ chow (n = 3), iWT HFD (n = 3), and *Atp7b*$^{\Delta IEC}$ HFD (n = 3). Abbreviation: HFD, high-fat diet.

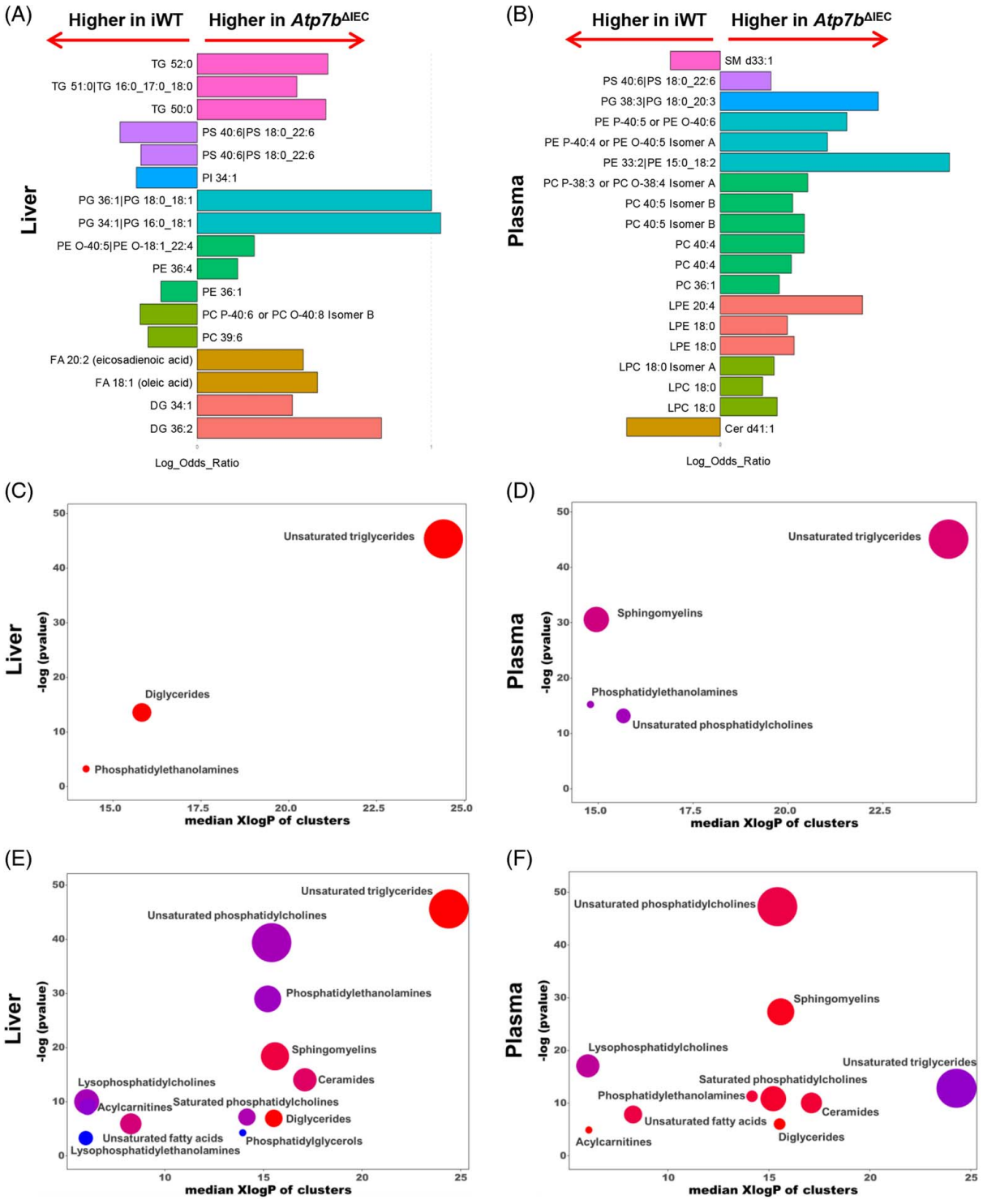

FIGURE 6 Lipidomic profile in liver and in plasma of *Atp7b*$^{\Delta IEC}$ mice fed chow or HFD. (A, B) Linear discriminant analysis effect size (LEfSe) plots representing the logarithm of the average level ratios of statistically different lipids between *Atp7b*$^{\Delta IEC}$ and WT mice on chow in liver and plasma. A positive log ratio bar indicates higher lipid levels in *Atp7b*$^{\Delta IEC}$ mice; a negative log ratio bar indicates higher levels in iWT mice. Colors represent lipids in the same class. (C, D) Chemical similarity enrichment analysis (ChemRICH) and enrichment statistics plot for *Atp7b*$^{\Delta IEC}$ HFD versus iWT HFD mice in liver and plasma. Each cluster represents an altered chemical class of metabolites ($p < 0.05$). Cluster size represents the total number of metabolites. Cluster color represents the directionality of metabolite differences: red, higher in *Atp7b*$^{\Delta IEC}$ HFD mice; blue, lower in *Atp7b*$^{\Delta IEC}$ chow mice. Colors in between refer to a mixed population of metabolites manifesting both higher and lower levels in *Atp7b*$^{\Delta IEC}$ HFD when compared with iWT HFD. The *x*-axis represents the cluster order on the chemical similarity tree. The *y*-axis represents chemical enrichment *p*-values calculated using Kolmogorov-Smirnov test. (E, F) ChemRICH and enrichment statistics plot for *Atp7b*$^{\Delta IEC}$ HFD versus *Atp7b*$^{\Delta IEC}$ chow mice in liver and plasma. iWT chow (n = 7), *Atp7b*$^{\Delta IEC}$ chow (n = 8), iWT HFD (n = 8), and *Atp7b*$^{\Delta IEC}$ HFD (n = 8). Abbreviations: FA, fatty acid; PC, phosphatidylcholine; PE, phosphatidylethanolamine; TAG, triacylglycerides; LPC, lysophosphatidylcholines.

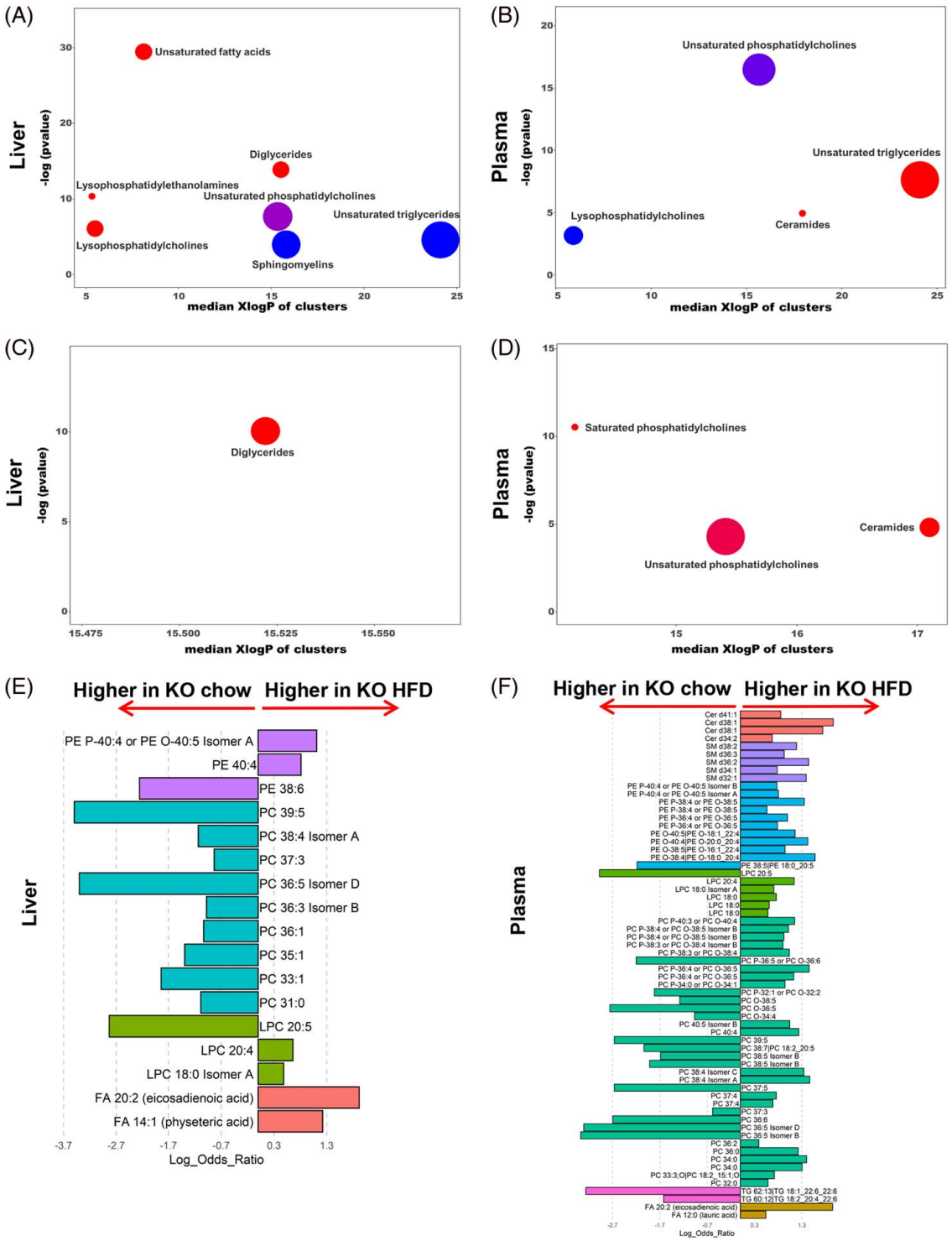

FIGURE 7 Lipidomic profiles in liver and plasma of KO mice fed chow or HFD. (A, B) Chemical similarity enrichment analysis (ChemRICH) and enrichment statistics plot for KO HFD versus WT HFD mice in liver and plasma. Each cluster represents an altered chemical class of metabolites ($p < 0.05$). Cluster size represents the total number of metabolites. Cluster color represents the directionality of metabolite differences: red, higher in KO HFD mice. The *x*-axis represents the cluster order on the chemical similarity tree. The *y*-axis represents chemical enrichment *p*-values calculated using a Kolmogorov-Smirnov test. (C, D) ChemRICH and enrichment statistics plot for KO HFD versus KO chow mice in liver and plasma. (E, F) Linear discriminant analysis effect size (LEfSe) plots representing the logarithm of the ratios of the average levels of statistically different lipids between KO HFD and KO chow mice in liver and plasma. A positive log ratio bar indicates higher lipid levels in KO HFD; a negative log ratio bar indicates higher levels in KO chow mice. Colors represent lipids in the same class. WT chow (n = 3), KO chow (n = 3), WT HFD (n = 3), and KO HFD (n = 4). Abbreviations: HFD, high-fat diet; KO, knockout; PC, phosphatidylcholine; PE, phosphatidylethanolamine;

alterations in the microbiome and lipidome of WD mouse models were highly correlated with microbiome functional analyses, supporting a role for gut flora composition in WD metabolic complications. Last, we demonstrated a novel mechanism with a potential role in WD pathogenesis in which intestine-specific *ATP7B* deficiency resulted in changes in IEC transcriptome and a diet-dependent dysregulation of the lipidome independent of hepatic copper accumulation, gut microbiome profile, and advanced liver disease.

Previous studies have shown decreased gut microbiome diversity in WD patients compared to healthy subjects with a higher abundance of Bacteroidetes and lower abundance of Firmicutes, Proteobacteria, and Fusobacteria.[18] Notably, our study supports previous findings in patients and confirms reduced intestinal flora diversity in animal models of WD, independent of advanced liver disease, which influences microbiome composition. In particular, we show genus level changes including a higher abundance of *Mucispirillum*, *Lactobacillus*, *Rikenellaceae RC9* gut group, *Muribaculum*, *Odoribacter*, and *Oscillibacter*, and lower abundance of *Helicobacter*, *Blautia*, and *Bilophila* in tx-j compared with C3H control mice. Decreased *Bifidobacterium* and *Bacteroides*, and increased *Desulfovibrionaceae*, *Anaerotruncus*, *Desulfovibrio*, and *Mucispirillum* were previously reported in high-cholesterol diet-induced NAFLD-HCC animals along with decreased 3-indolepropionic acid.[19] We have previously described dysregulated hepatic cholesterol homeostasis [1] and reduced 3-indolepropionic acid [4] in WD. The positive correlation between *Mucispirillum*, *Muribaculum*, and *Odoribacter*, and hepatic steatosis, oxidative stress, and inflammation in alcohol-associated liver disease [20] as well as the association of *Bilophila*, *Paraprevotella*, and *Suturella* with higher hepatic fat content [21] implicate these microbial genera in hepatic pathological manifestations in WD. Besides low microbial diversity, we show WD is associated with major compositional shift. Accumulating evidence supports the gut microbiota playing a role in modulating host metabolism.[22] Notably, our findings from the functional metagenome analysis indicate an enrichment of genera involved in energy metabolism, including amino acid, carbohydrate, and lipid metabolisms. This is in agreement with a previous study on dietary copper supplementation in pigs, which showed a decreased abundance of microbiota related to energy metabolism, for example, lysine and other amino acid biosynthesis, and an increased abundance of microbiota related to amino acid and lipid biosynthesis and metabolism.[23] Our findings imply that the observed microbiota alterations are connected with alterations in energy metabolism reported in WD;[24] however, specific mechanisms remain to be uncovered. As growing evidence indicates, WD is a multiorgan condition, with involved organs including the liver and the brain. Multiple factors affect hepatic pathology and neurologic conditions, including microbiome and phospholipid and sphingolipid metabolism derangements.[25] The gut microbiome was shown to affect phospholipid levels in germ-free mice,[26] and sphingolipids and ceramides were shown to be produced by specific phyla of the gut microbiome.[27] Therefore, the association observed between intestinal microbiota and many phospholipid and sphingolipid species suggests microbiome involvement in WD-associated liver and neurologic physiopathology. It is unclear why KO mice present more attenuated, albeit parallel, differences in microbiome and lipidome patterns compared to tx-j mice. We hypothesize global KO mice have developed compensatory mechanisms that might influence metabolic machinery already at 16 weeks of age or earlier.[28]

Whereas derangements in lipid metabolism are reported in patients with WD,[24] our findings highlight lipidomic dysregulation independent of advanced liver disease and hepatic copper accumulation. These include derangements in fatty acid desaturation and elongation pathways, with lower levels of many VLCFAs including behenic acid (22:0), erucic acid (22:1n9), and nervonic acid (24:1n9), which can originate from the denaturation and elongation of palmitic acid (16:0) and stearic acid (18:0). We also observed lower levels of several TAGs and PLs with unsaturated double bonds, suggesting a de-enrichment of monounsaturated and polyunsaturated fatty acids in these lipid classes. Our results corroborate previous reports from our group and others indicating lower activity/transcript levels or impaired function of nuclear receptors, for example, farnesoid X receptor, liver X receptors, and heterodimer with retinoid X receptor; transcription factors, for example, sterol regulatory element-binding protein (SREBP1c); and peroxisome-proliferator-activated receptor alpha (PPARα), which regulate lipogenic genes in both animal models and patients with WD.[29–34]

Our approach highlights lipidomic alterations that have been, at least in part, previously described in WD. We have reported altered SL metabolism in subjects with WD [10] and ceramide and sphingomyelin were found to be increased in patients with WD.[35] In the current analysis, liver and plasma SL profiles were altered with higher ceramide and altered sphingomyelin profiles. The involvement of aberrant ceramide metabolism in WD was shown *in vitro* and *in vivo*, with increased ceramide levels in WD.[36] The inhibition of ceramide production in a rat model of WD prevented the development of cirrhosis.[36] Evidence from animal studies indicates the role of ceramides in hepatic steatosis, inflammation, hepatocellular apoptosis, and fibrosis.[37] The hepatic and plasma PL profiles were also found altered, a feature reportedly associated with an increased risk of hepatic steatosis.[38] This finding is consistent with our previous work showing dysregulated serum PL profile in WD patients compared to healthy controls and downregulation of genes involved in PC

synthesis and metabolism, including PE N-methyltransferase (PEMT) and choline phosphotransferase1.[10]

A noteworthy correlation analysis highlighted the differentially abundant microbial genera; in particular, *Mucispirillum* and *Lactobacillus* were associated with alterations in PL and correlated negatively with many TAGs and SMs. *Mucispirillum* also correlated positively with ceramides. As current evidence indicates an association of gut microbiota composition with lipid profiles,[39] the association reported in our study suggests implications of these genera in the observed lipidomic alterations in WD mice.

Importantly, our data demonstrate the role of intestine ATP7B in modulating lipid metabolism independent from hepatic copper accumulation or severe hepatic pathological changes. We show that the intestinal ATP7B transporter deletion resulted in the mislocalization of APOB48 in the intestine which presented a diffuse pattern of cytosolic distribution only in *Atp7b*$^{\Delta IEC}$ mice after a HFD challenge. This pattern of distribution likely represents deficits in chylomicron processing and secretion with consequent accumulation of very-low-density lipoproteins within the IECs.[11] In addition, whereas we did not detect changes in gut microbiome and liver copper concentration in *Atp7b*$^{\Delta IEC}$ mice, these mice presented a specific IEC transcriptomic profile (with affected RNA synthesis machinery, epigenetic changes, and compound oxidation genes), altered plasma and liver lipidomic profiles, and initial changes in liver pathology. Ultimately, ATP7B intestine-specific deficiency was associated with diet-specific alterations in plasma and liver lipidomic profiles, only partially explained by genetic background. Specifically, the HFD challenge in *Atp7b*$^{\Delta IEC}$ resulted in similar changes to that seen in tx-j and KO mice, with lower nervonic acid (24:1n9) and palmitoleic acid (16:1n7), and an increase in several polyunsaturated fatty acids indicates altered fatty acid desaturation pathways.

HFD in *Atp7b*$^{\Delta IEC}$ mice also resulted in decreased plasma TAGs, possibly explained by impaired intestinal lipid absorption; increased hepatic TAG and DG, possibly due to increased hepatic *de novo* synthesis; and altered hepatic PLs and SLs. Our findings suggest intestinal ATP7B directly affects and is a diet-dependent modulator of lipid metabolism. This highlights a novel potential mechanism to explain WD pathogenesis and associated dysregulations in lipid metabolism that points to the involvement of extrahepatic organs. The implications of altered intestinal ATP7B and lipidomic profile build upon a pattern of lipid changes after a high-fat diet that differs from the pattern previously observed in primary hepatocytes isolated from C57BL/6 mice after a 6-week course of 45% fat diet, which was characterized mostly by PC, LPC, and DG increase with TG stability, as identified by lipidomic analysis.[40] A 60% fat diet provided for 12 weeks to C57BL/6 mice was associated with TG increase and reduction of PC, LPC, and PE [41] with less marked changes in SM and ceramides.

The *Atp7b*$^{\Delta IEC}$ mice studied here is a new model with limited metabolic characterization thus far and which was studied only at early time points. In addition, the use of a germ-free facility and long-term HFD will likely aid in disentangling the exact role of the gut microbiome on metabolic changes. Regardless, it was important to define the role of a short-course challenge on metabolic derangements and this short-course challenge will have to be compared to long-term studies.[9] Despite these limitations, we used a multiomics approach to show that ATP7B deficit in 2 mouse models of WD results in alterations in the microbiome and lipidome, with dysregulation affecting fatty acid desaturation pathways and SL metabolism further augmented by HFD. Notably, we observed consistent increases in ceramide levels that were exacerbated by the HFD challenge, pointing to an increased risk of chronic liver damage. These findings support the role of diet and the implication of these pathways in WD progression.

Altogether, our data points to hitherto unstudied interconnectivity of organs and the microbiome resulting in changes typically associated with WD pathogenesis and related metabolic changes. Through observations in 3 mouse models, we demonstrate changes in metabolic pathways associated with changes in lipid profiles and microbiome alterations. The changes highlight the importance of copper homeostasis in systemic energy production.

Our study also highlights a role for extrahepatic ATP7B specifically modulating lipid metabolism in WD pathogenesis shown to be dependent on diet but independent from severe liver disease and hepatic copper accumulation. Gut microbiome is also connected to lipid metabolism but these effects are apparent only when there is hepatic copper accumulation. Ultimately, the interplay between copper accumulation and lipid metabolism as shown by -omic profiles underscores the complexity of WD and indicates WD should be considered a systemic disease where energy and lipid metabolism interact at an organ-specific level to modulate the phenotypic presentation.

FUNDING INFORMATION

This work was supported by the UC Davis Microbiome Special Research Program and UC Davis Gastroenterology Division funds (to Valentina Medici), The National Institutes of Health (NIH) by R01 DK104770 (to Valentina Medici), R01 AA027075 (to Janine M. LaSalle), R01 DK071865 (to Svetlana Lutsenko), and the Deputyship for Research and Innovation, Ministry of Education of Saudi Arabia by IFKSUOR3–199-1 (to Tagreed A. Mazi). The project described was supported by the National Center for Advancing Translational Sciences, National Institutes of Health, through grant number UL1 TR001860. The content is solely the responsibility of the authors and does not necessarily represent the official views of the NIH.

CONFLICTS OF INTEREST

Valentina Medici serves on the Advisory Board of Alexion Pharmaceuticals, Arbormed, and Orphalan. The remaining authors have no conflicts to report.

ORCID

Tagreed A. Mazi https://orcid.org/0000–0002–1250–723
Kari Neier https://orcid.org/0000–0002–9700–4045
Marie C. Heffern https://orcid.org/0000–0001–7501–2741
Maneesh Dave https://orcid.org/0000–0002–4068–6700
Janine M. LaSalle https://orcid.org/0000–0002–3480–2031
Svetlana Lutsenko https://orcid.org/0000–0001–5275–2587

REFERENCES

1. Sarode GV, Neier K, Shibata NM, Shen Y, Goncharov DA, Goncharova EA, et al. Wilson disease: intersecting DNA methylation and histone acetylation regulation of gene expression in a mouse model of hepatic copper accumulation. Cell Mol Gastroenterol Hepatol. 2021;12:1457–77.
2. Hamilton JP, Koganti L, Muchenditsi A, Pendyala VS, Huso D, Hankin J, et al. Activation of liver X receptor/retinoid X receptor pathway ameliorates liver disease in Atp7B(-/-) (Wilson disease) mice. Hepatology. 2016;63:1828–41.
3. Einer C, Leitzinger C, Lichtmannegger J, Eberhagen C, Rieder T, Borchard S, et al. A high-calorie diet aggravates mitochondrial dysfunction and triggers severe liver damage in Wilson disease rats. Cell Mol Gastroenterol Hepatol. 2019;7:571–96.
4. Sarode GV, Kim K, Kieffer DA, Shibata NM, Litwin T, Czlonkowska A, et al. Metabolomics profiles of patients with Wilson disease reveal a distinct metabolic signature. Metabolomics. 2019;15:43.
5. Mazi TA, Sarode GV, Czlonkowska A, Litwin T, Kim K, Shibata NM, et al. Dysregulated choline, methionine, and aromatic amino acid metabolism in patients with Wilson disease: exploratory metabolomic profiling and implications for hepatic and neurologic phenotypes. Int J Mol Sci. 2019;20:5937.
6. Harder NHO, Hieronimus B, Stanhope KL, Shibata NM, Lee V, Nunez MV, et al. Effects of dietary glucose and fructose on copper, iron, and zinc metabolism parameters in humans. Nutrients. 2020;12:2581.
7. Muchenditsi A, Talbot CC, Gottlieb A, Yang H, Kang B, Boronina T, et al. Systemic deletion of Atp7b modifies the hepatocytes' response to copper overload in the mouse models of Wilson disease. Scientific Reports. 2021;11:5659.
8. Huster D, Purnat TD, Burkhead JL, Ralle M, Fiehn O, Stuckert F, et al. High copper selectively alters lipid metabolism and cell cycle machinery in the mouse model of Wilson disease. J Biol Chem. 2007;282:8343–55.
9. Wooton-Kee CR, Robertson M, Zhou Y, Dong B, Sun Z, Kim KH, et al. Metabolic dysregulation in the Atp7b(-/-) Wilson's disease mouse model. Proc Natl Acad Sci USA. 2020;117:2076–83.
10. Mazi TA, Sarode GV, Czlonkowska A, Litwin T, Kim K, Shibata NM, et al. Dysregulated choline, methionine, and aromatic amino acid metabolism in patients with Wilson disease: exploratory metabolomic profiling and implications for hepatic and neurologic phenotypes. Int J Mol Sci. 2019;20:5937.
11. Pierson H, Muchenditsi A, Kim BE, Ralle M, Zachos N, Huster D, et al. The function of ATPase copper transporter ATP7B in intestine. Gastroenterology. 2018;154:168–80.e165.
12. Cai X, Deng L, Ma X, Guo Y, Feng Z, Liu M, et al. Altered diversity and composition of gut microbiota in Wilson's disease. Sci Rep. 2020;10:21825.
13. Muchenditsi A, Yang H, Hamilton JP, Koganti L, Housseau F, Aronov L, et al. Targeted inactivation of copper transporter Atp7b in hepatocytes causes liver steatosis and obesity in mice. Am J Physiol. 2017;313:G39–49.
14. Medici V, Shibata NM, Kharbanda KK, LaSalle JM, Woods R, Liu S, et al. Wilson's disease: changes in methionine metabolism and inflammation affect global DNA methylation in early liver disease. Hepatology. 2013;57:555–65.
15. Le A, Shibata NM, French SW, Kim K, Kharbanda KK, Islam MS, et al. Characterization of timed changes in hepatic copper concentrations, methionine metabolism, gene expression, and global DNA methylation in the Jackson toxic milk mouse model of Wilson disease. Int J Mol Sci. 2014;15:8004–23.
16. Buiakova OI, Xu J, Lutsenko S, Zeitlin S, Das K, Das S, et al. Null mutation of the murine ATP7B (Wilson disease) gene results in intracellular copper accumulation and late-onset hepatic nodular transformation. Hum Mol Genet. 1999;8:1665–71.
17. Roberts EA, Robinson BH, Yang S. Mitochondrial structure and function in the untreated Jackson toxic milk (tx-j) mouse, a model for Wilson disease. Mol Genet Metab. 2008;93:54–65.
18. Geng H, Shu S, Dong J, Li H, Xu C, Han Y, et al. Association study of gut flora in Wilson's disease through high-throughput sequencing. Medicine (Baltimore). 2018;97:e11743.
19. Zhang X, Coker OO, Chu ES, Fu K, Lau HCH, Wang YX, et al. Dietary cholesterol drives fatty liver-associated liver cancer by modulating gut microbiota and metabolites. Gut. 2021;70:761–74.
20. Tian X, Li R, Jiang Y, Zhao F, Yu Z, Wang Y, et al. Bifidobacterium breve ATCC15700 pretreatment prevents alcoholic liver disease through modulating gut microbiota in mice exposed to chronic alcohol intake. J Funct Foods. 2020;72:104045.
21. Philips CA, Augustine P, Yerol PK, Ramesh GN, Ahamed R, Rajesh S, et al. Modulating the intestinal microbiota: therapeutic opportunities in liver disease. J Clin Transl Hepatol. 2020;8:87–99.
22. Aron-Wisnewsky J, Warmbrunn MV, Nieuwdorp M, Clément K. Metabolism and metabolic disorders and the microbiome: the intestinal microbiota associated with obesity, lipid metabolism, and metabolic health-pathophysiology and therapeutic strategies. Gastroenterology. 2021;160:573–99.
23. Zhang Y, Zhou J, Dong Z, Li G, Wang J, Li Y, et al. Effect of dietary copper on intestinal microbiota and antimicrobial resistance profiles of Escherichia coli in weaned piglets. Front Microbiol. 2019;10:2808.
24. Mazi TA, Shibata NM, Medici V. Lipid and energy metabolism in Wilson disease. Liver Research. 2020;4:5–14.
25. Paul B, Lewinska M, Andersen JB. Lipid alterations in chronic liver disease and liver cancer. JHEP Rep. 2022;4:100479.
26. Velagapudi VR, Hezaveh R, Reigstad CS, Gopalacharyulu P, Yetukuri L, Islam S, et al. The gut microbiota modulates host energy and lipid metabolism in mice. J Lipid Res. 2010;51:1101–2.
27. Johnson EL, Heaver SL, Waters JL, Kim BI, Bretin A, Goodman AL, et al. Sphingolipids produced by gut bacteria enter host metabolic pathways impacting ceramide levels. Nat Commun. 2020;11:2471.
28. Medici V, Huster D. Animal models of Wilson disease. Handb Clin Neurol. 2017;142:57–70.
29. Medici V, Shibata NM, Kharbanda KK, LaSalle JM, Woods R, Liu S, et al. Wilson's disease: changes in methionine metabolism and inflammation affect global DNA methylation in early liver disease. Hepatology. 2013;57:555–65.
30. Huster D, Purnat TD, Burkhead JL, Ralle M, Fiehn O, Stuckert F, et al. High copper selectively alters lipid metabolism and cell cycle machinery in the mouse model of Wilson disease. J Biol Chem. 2007;282:8343–55.

31. Wooton-Kee CR, Jain AK, Wagner M, Grusak MA, Finegold MJ, Lutsenko S, et al. Elevated copper impairs hepatic nuclear receptor function in Wilson's disease. J Clin Invest. 2015;125:3449–60.
32. Wilmarth PA, Short KK, Fiehn O, Lutsenko S, David LL, Burkhead JL. A systems approach implicates nuclear receptor targeting in the Atp7b−/− mouse model of Wilson's disease. Metallomics. 2012;4:660–8.
33. Hamilton JP, Koganti L, Muchenditsi A, Pendyala VS, Huso D, Hankin J, et al. Activation of liver X receptor/retinoid X receptor pathway ameliorates liver disease in Atp7B−/−(Wilson disease) mice. Hepatology. 2016;63:1828–41.
34. Nagasaka H, Miida T, Inui A, Inoue I, Tsukahara H, Komatsu H, et al. Fatty liver and anti-oxidant enzyme activities along with peroxisome proliferator-activated receptors γ and α expressions in the liver of Wilson's disease. Mol Genet Metab. 2012;107:542–7.
35. Zhi Y, Sun Y, Jiao Y, Pan C, Wu Z, Liu C, et al. HR-MS based untargeted lipidomics reveals characteristic lipid signatures of Wilson's disease. Front Pharmacol. 2021;12:754185.
36. Lang PA, Schenck M, Nicolay JP, Becker JU, Kempe DS, Lupescu A, et al. Liver cell death and anemia in Wilson disease involve acid sphingomyelinase and ceramide. Nat Med. 2007;13:164–70.
37. Poss AM, Summers SA. Too much of a good thing? An evolutionary theory to explain the role of ceramides in NAFLD. Front Endocrinol (Lausanne). 2020;11:505.
38. van der Veen JN, Kennelly JP, Wan S, Vance JE, Vance DE, Jacobs RL. The critical role of phosphatidylcholine and phosphatidylethanolamine metabolism in health and disease. Biochimica et Biophysica Acta. 2017;1859:1558–72.
39. Schoeler M, Caesar R. Dietary lipids, gut microbiota and lipid metabolism. Rev Endocr Metab Disord. 2019;20:461–72.
40. Chitraju C, Trötzmüller M, Hartler J, Wolinski H, Thallinger GG, Lass A, et al. Lipidomic analysis of lipid droplets from murine hepatocytes reveals distinct signatures for nutritional stress. J Lipid Res. 2012;53:2141–52.
41. Kim SQ, Mohallem R, Franco J, Buhman KK, Kim K-H, Aryal UK. Multi-omics approach reveals dysregulation of protein phosphorylation correlated with lipid metabolism in mouse non-alcoholic fatty liver. Cells. 2022;11:1172.

How to cite this article: Sarode GV, Mazi TA, Neier K, Shibata NM, Jospin G, Harder NH, et al. The role of intestine in metabolic dysregulation in murine Wilson disease. Hepatol Commun. 2023;7:e0247. https://doi.org/10.1097/HC9.0000000000000247